

Anisotropic Cage Evolution in Quasi-two-dimensional Colloidal Fluids

Noman Hanif Barbhuiya¹ and Chandan K. Mishra^{1,*}

¹*Department of Physics, Indian Institute of Technology Gandhinagar, Palaj, Gandhinagar, 382055, Gujarat, India*

(Dated: July 26, 2024)

Employing video microscopy, we explore the cage dynamics for colloidal particles confined in quasi-two dimensions (q2D). Our experiments reveal that while ensemble-averaged dynamics of cages are isotropic in the laboratory frame, its evolution in the displacement frame of the caged particle is anisotropic and asymmetric. In turn, this leads to particles in specific regions of the cage contributing either to cage persistence or breaking, influencing the structural relaxation of the fluid. Our findings, thus, provide microscopic insights into cage evolution and dynamics for colloidal fluids in q2D, with direct potential implications for the flow of complex fluids, structural relaxation in dense suspensions, and collective motion in active matter in confined geometries.

Cage formation, whether transient or long-lived, is a fundamental feature of condensed matter systems such as (supercooled) liquids [1–4], glasses [5–8] and crystals [9–12]. Microscopic insights into the structural configuration and dynamical evolution of cages have offered crucial understandings of diverse phenomena, such as the rheological [13] and mechanical properties [5] of the materials as well as their phase behavior [14]. For example, while the shape and geometry of the cage can distinguish between supercooled liquid and glassy states of passive glass formers [15], the cage length and persistence elucidate the phase behavior of active glasses [14]. Notably, the distinct nature of glass transition and melting of crystal in reduced spatial dimensions like two-dimensions (2D), compared to three-dimensions (3D), wherein long-wavelength Mermin-Wagner fluctuations influence the dynamics, have become dimension-agnostic once the dynamics of the particles relative to its cage, instead of their self-dynamics, are considered [16–18].

Interestingly, recent studies suggest that long-wavelength Mermin-Wagner fluctuations are also present in 2D colloidal liquids, leading to the violation of the ubiquitous Stokes-Einstein relation, which connects the microscopic diffusivity of the tracers and the bulk viscosity of the liquid. Once again, the cage-relative dynamics of the particles have been shown to restore the usual behavior of the Stokes-Einstein relation for 2D liquids [19]. However, despite the extensive exploration of cage relative dynamics, the evolution of the cages themselves in 2D colloidal fluids – their transient nature leading to possible changes in their shape over time, which consequently dictates the local structural relaxation of the fluid – has never been explored. It is particularly intriguing as long-wavelength fluctuations have been alluded to stem from hydrodynamic interactions [19, 20], which have been revealed to be direction-dependent in the body frame of particle-pair for quasi-two-dimensional (q2D) colloidal fluids [21]. The influence of these emergent hydrodynamic interactions in q2D colloidal fluids on the dynamic evolution of the cages is anything but obvious.

In this Letter, we employ video microscopy to exper-

imentally investigate the temporal evolution of cages, both in the laboratory and in the displacement frame of the reference caged-colloid in q2D colloidal fluids. The cage of each particle at the initial time, t_0 , is determined using its Voronoi cell [15]. As expected, with time, the size of the cages grows, leading to the local structural relaxation of the fluid [Figure 1] [22, 23]. Interestingly, ensemble-averaged dynamics of particles forming the cage reveal that while they diffuse isotropically in the laboratory frame of reference, the distribution of the particles forming the cage is observed to be anisotropic and asymmetric in the displacement frame of the caged-particle [Figure 2]. Finally, consistent with dipolar hydrodynamic motional modes, we identify distinct hotspots for particles of the cage at the initial time that either contribute to cage persistence or cage relaxation at a later time and demonstrate their anisotropic evolution [Figure 3].

Aqueous suspension of charge-stabilized polystyrene colloidal particles, diameter: $\sigma = 1.04 \mu\text{m}$, polydispersity $\sim 3\%$, were loaded in a wedge-shaped cell, which was then allowed to stand vertically for particles to sediment under gravity and form a monolayer in the quasi-two-dimensional region of the cell [21]. Once a desired area fraction was achieved, the cell was equilibrated for several hours under the microscope. After equilibration, video microscopy was performed for 20 minutes using 100x oil objective (1.4 Numerical aperture) at 10 frames per second (fps) using the Hamamatsu ORCA-Flash4.0 camera. We have captured data in the liquid regime at five area fractions, ϕ , in the range, $0.15 \leq \phi \leq 0.35$, in the same region of the cell. The trajectory of each particle was determined using standard image processing and tracking algorithms [24]. The dynamic spatial resolution in our experiment was 20 nm.

The identity of cage particles, $C(i, t)$, for i^{th} -particle at time, t , is determined using Voronoi tessellation, which partitions the 2D space into neighborhoods (cells) around each particle such that every point within a cell is closer to the particle than to any other particle [inset to Fig. 1(a)] [25]. The order of $C(i, t)$, $n(C(i, t))$, represents the number of particles forming the cage of the i^{th} -particle

that is also equal to the number of vertices in its Voronoi cell. With time, the identity of particles contained in $C(i, t)$ changes, leading to the relaxation of the cage and, consequently, the local structural relaxation of the fluid. The relaxation (or persistence) time of the cage is measured by calculating the ensemble-averaged fraction of common cage particles, $\langle f(\Delta t) \rangle$, with lag time, Δt , $\langle f(\Delta t) \rangle = \frac{1}{N} \langle \sum_i \frac{n(C(i, t_0) \cap C(i, t_0 + \Delta t))}{n(C(i, t_0))} \rangle_{t_0}$. Here, $\langle \cdot \rangle_{t_0}$ represents initial time averaging over t_0 , corresponding to a given Δt , and N is the total number of particles. $\langle f(\Delta t) \rangle$ exhibits a stretched-exponential decay and yields the persistence time of the cage [Fig. 1(a)]. For the range of ϕ s studied, the persistence time was observed to be around 10 s, which is comparable to the timescales over which effects of hydrodynamics are conspicuous. Thus, the cage evolution and dynamics may be closely connected to the local structural relaxation of the fluid governed by hydrodynamic interactions.

Moreover, as the local structure of the fluid relaxes, the particles of the cage will randomly diffuse, leading to an increase in average cage size, which can be measured using the radius of gyration, $R_g(i, \Delta t)$, of the particles forming the cage of i^{th} -particle over Δt . $R_g(i, \Delta t) =$

$$\sqrt{\frac{1}{n(C(i, \Delta t))} \sum_{c_j \in C(i, \Delta t)} (\mathbf{r}_j(t_0 + \Delta t) - \langle \mathbf{r}_j(t_0 + \Delta t) \rangle_j)^2}.$$

Here, $\mathbf{r}_j(t_0 + \Delta t)$ is the position of the j^{th} -particle belonging to the set of particles that form the cage of i^{th} -particle at t_0 . Note, throughout the Letter, the sets and their elements are represented using upper and lowercase letters, respectively. The ensemble-averaged distribution of $R_g(i, \Delta t)$, $R_g(\Delta t)$, is found to be Gaussian [inset to Fig. 1(b)]. As expected, $R_g(\Delta t)$ grows with Δt . Over the persistent time of the cages (~ 10 s), it is found to be about $2\text{-}3\sigma$ [Fig. 1(b)], implying that the temporal evolution of cages should be strongly governed by the nature of near-field hydrodynamic interactions in q2D spatial confinement, which is direction-dependent (anisotropic) in the body frame of colloid-pairs [21].

As the fluid relaxes, particles of the cage, as defined at t_0 , will also diffuse, which may lead to a change in the shape of the cage. Thus, to capture the microscopic evolution in the shape of the cages with Δt , we plot the probability distribution, $P(\mathbf{r}_j(t_0 + \Delta t) | c_j \in C(i, t_0))$, of the positions of the particles of the cage, defined at t_0 , over Δt [Fig. 2(a)-(e)]. Here, the argument on the right of the “|” represents the condition applied for the quantity being measured on the left. Note that the probabilities are calculated from the ensembles of particles (and their cages) and averaged over Δt . Particles forming the cage spread radially, both outward and inward, from their initial position, with $P(\mathbf{r}_j(t_0 + \Delta t) | c_j \in C(i, t_0))$ being symmetric about the center of mass of the cages at t_0 . The diffused annular ring signifies the caging of the particle by its neighbors in colloidal fluids [Fig. 2(b)-(e)], and as

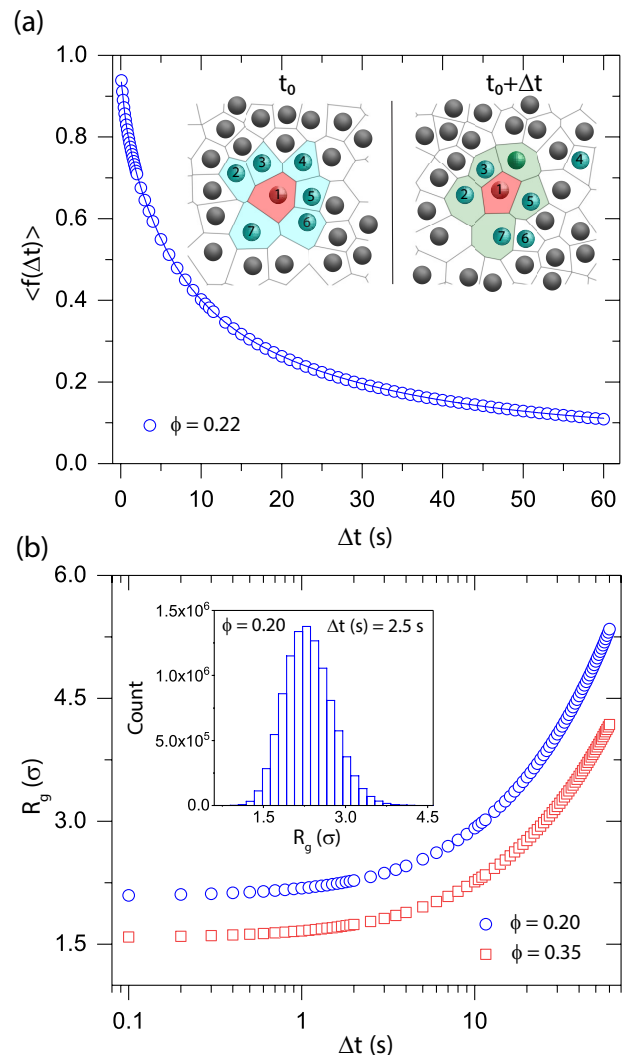


FIG. 1. Cage characterization in quasi-two-dimensional colloidal fluids. (a) Average fraction of common cage particles, $\langle f(\Delta t) \rangle$, versus lag time, Δt , for area fraction, $\phi = 0.22$. Inset shows the rendering of the Voronoi cells (polygons) for a representative subset of particles (spheres) in the experimental field of view at initial, t_0 (left), and later time, $t_0 + \Delta t$ (right). The representative reference particle's (red sphere) Voronoi cell with its adjoining cells at t_0 (cyan polygons) and $t + \Delta t$ (green polygons), determines the identity of the particles forming the cage (shown as numerals on the spheres). (b) The average radius of gyration, $R_g(\Delta t)$, of the particles forming the cage versus lag time, Δt , for $\phi = 0.20$ (blue circles) and $\phi = 0.35$ (red squares). The inset shows the distribution of R_g for $\phi = 0.20$ at $\Delta t = 2.5$ s.

expected, the annular ring spreads with Δt . For a given Δt , with an increase in ϕ , as caging effects strengthen, the annular ring becomes more localized [Fig. 2(b)-(i) & Supplemental Video 1].

$P(\mathbf{r}_j(t_0 + \Delta t) | c_j \in C(i, t_0))$ is found to be symmetric. However, note that the laboratory frame of measurements of the positions of particles forming the cage for

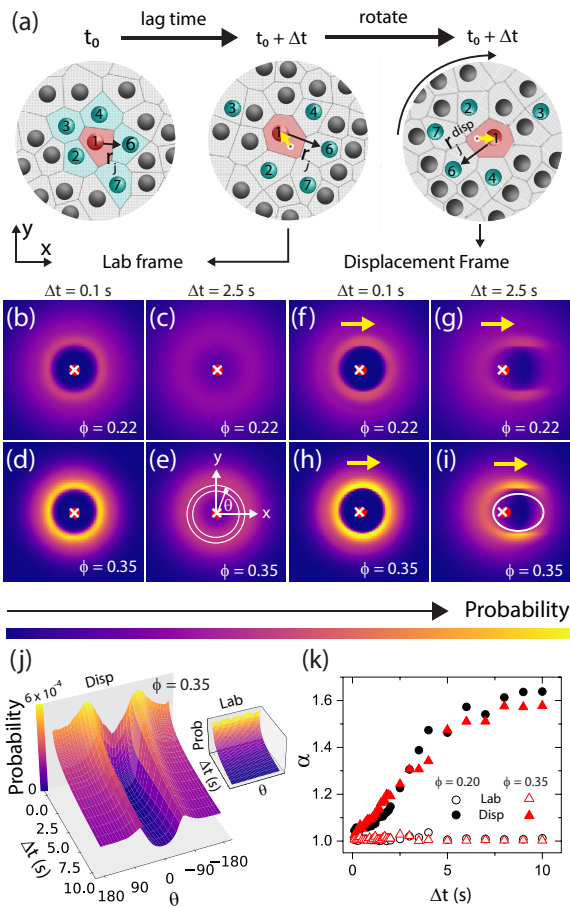


FIG. 2. Cage evolution in quasi-two-dimensional colloidal fluids. (a) Rendering from experiments illustrating the laboratory and displacement frames of reference. A portion of the field of view at times t_0 (left) and $t_0 + \Delta t$ (middle), a representative particle (red sphere) and its cage particles (cyan spheres) are determined from Voronoi cells (cyan polygons) at t_0 . The right panel demonstrates the transformation of particle coordinates to the displacement frame, where the displacement of the reference-caged particle (red) is aligned with the x -axis. Ensemble-averaged colormap of the probability distribution of the positions of the particles forming the cage, $P(\mathbf{r}_j(t_0 + \Delta t)|c_j \in C(i, t_0))$, in the (b)-(e) laboratory frame, and (f)-(i) displacement frame, $P(\mathbf{r}_j^{disp}(t_0 + \Delta t)|c_j \in C(i, t_0))$, from all reference particles, for two distinct ϕ and Δt . The white cross and red solid circle in (b)-(i) represent the mean of the probability distribution at t_0 and $t_0 + \Delta t$, respectively. The yellow arrows in (g)-(i) show the displacement direction of the reference caged particle. (j) The net probability within an annular region with an inner and outer radius of 1σ and 1.25σ , centered on the mean of the probability distribution, as a function of angle θ with respect to the x -axis (as illustrated in (e)) and Δt for $\phi = 0.35$, in the displacement frame (main subfigure) and laboratory frame (inset). (k) The aspect ratio, α , of the fitted ellipse along the inner edge of the annular space of the probability distribution as a function of Δt for $\phi = 0.20$ (blue circles) and $\phi = 0.35$ (red triangle) in the laboratory (open symbols) and displacement frames (solid symbols).

the analysis of $P(\mathbf{r}_j(t_0 + \Delta t)|c_j \in C(i, t_0))$ will be unable to capture any possible influence of the unique nature of hydrodynamic interactions in q2D colloidal fluids on the evolution of the shape of the cages. Hence, to discern the effects of hydrodynamics on the evolution of the shape of the cages, we calculate $P(\mathbf{r}_j^{disp}(t_0 + \Delta t)|c_j \in C(i, t_0))$ in the displacement frame of the i^{th} -reference particle. Here, we rotate the positions of all the particles of the cages such that the displacement of reference-caged particle aligns along the x -axis [Fig. 2(a)]. In essence, we transform \mathbf{r}_i in the lab frame to \mathbf{r}_i^{disp} in displacement frame by $\mathbf{r}_i^{disp} = \mathbf{R}(-\psi)\mathbf{r}_i$, where ψ is angle that the displacement of the reference-caged particle subtends with x -axis and $\mathbf{R}(-\psi)$ is the rotation matrix with elements $R_{lm}(\psi) = \cos(\psi)\delta_{lm} + \sin(\psi)\delta_{lm}$.

Interestingly, unlike $P(\mathbf{r}_j(t_0 + \Delta t)|c_j \in C(i, t_0))$, $P(\mathbf{r}_j^{disp}(t_0 + \Delta t)|c_j \in C(i, t_0))$ deviates from the symmetric annular shape and is no longer isotropic with some preferred regions with higher probability density [Fig. 2(f)-(i) & Supplemental Video 2]. To quantify this localization of the probabilities, we calculate the net probability within an annular region with an inner and outer radius of 1σ and 1.25σ , which is centred on the mean of the probability distribution, as a function of angle θ (for example, see Fig. 2(e)). For a fixed ϕ , while the net probability is constant for all θ for $P(\mathbf{r}_j(t_0 + \Delta t)|c_j \in C(i, t_0))$, however, it displays two maxima at $\theta \sim \pm 90$ for $P(\mathbf{r}_j^{disp}(t_0 + \Delta t)|c_j \in C(i, t_0))$ [Fig. 2(j)]. It indicates an accumulation of particles forming the cage in regions perpendicular to the motion of the caged particle, which is in concordance with the dipolar nature of hydrodynamics in q2D colloidal fluid.

To further quantify the anisotropy in $P(\mathbf{r}_j^{disp}(t_0 + \Delta t)|c_j \in C(i, t_0))$, we fit an ellipse along the inner edge of the annular space, which outlines the contour of the probability distribution's maxima [26]. We define the aspect ratio of the fitted ellipsoid, α , the ratio of the major to the minor axis, as the anisotropy parameter associated with the probability distribution. In the laboratory frame, irrespective of the ϕ and Δt , α remains closer to unity, suggesting the isotropic spread of the particles of the cages around the reference caged-particle [Fig. 2(k)]. However, intriguingly, in the displacement frame, as already visually inferred from the colormaps in Figure 2(f)-(i), the shape anisotropy parameter α increases with Δt . The angle-dependent localization of $P(\mathbf{r}_j^{disp}(t_0 + \Delta t)|c_j \in C(i, t_0))$ and its time-dependent elongation, thus suggests a strong role of hydrodynamics governing the evolution of cages, potentially dictating the dynamics of cage breaking (and persistence).

Finally, having established that the shape of the cage is anisotropic in the displacement frame of the reference caged-particle, we now delve into how the particles of the cage rearrange, which either leads to the persistence of the cage or its breaking and local struc-

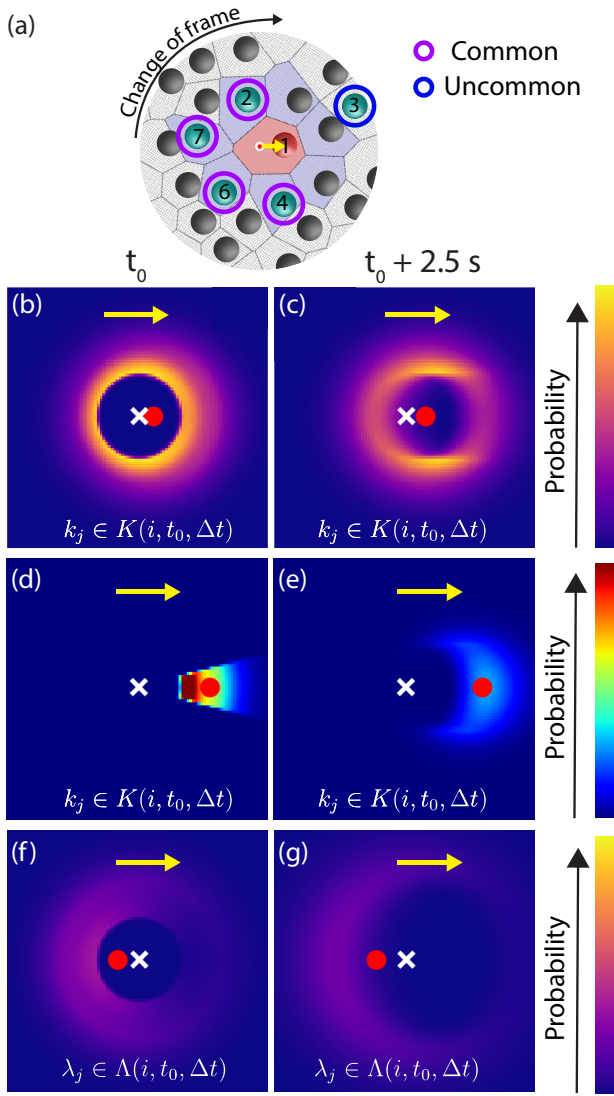


FIG. 3. Distinct anisotropic spatial probability distribution of the cage particles leading to cage persistence and relaxation. (a) Rendering from the experiments of a portion of the field of view illustrating the classification of cage particles (cyan spheres) at time t_0 into common, $K(i, t_0, \Delta t)$, and uncommon, $\Lambda(i, t_0, \Delta t)$, subsets based on their presence or absence in the cage defined for the same reference particle (red sphere) a later time, $t_0 + \Delta t$. The common and uncommon cage particles are circled in purple and blue, respectively. (b) Colormap of the probability distribution of the positions of the common cage particles, $P(\mathbf{r}_j^{disp}(t_0)|k_j \in K(i, t_0, \Delta t))$ and (c) $P(\mathbf{r}_j^{disp}(t_0 + \Delta t)|k_j \in K(i, t_0, \Delta t))$, at t_0 and $t_0 + \Delta t$, respectively, for $\phi = 0.35$ and $\Delta t = 2.5$ s. (d) and (e) show the probability distribution of the positions of the common cage particles at t_0 and $t_0 + \Delta t$, respectively, for $\phi = 0.35$ and $\Delta t = 2.5$ s, considering only the subset of particles within an angular region of $\pm 15^\circ$ with respect to the direction of displacement of the reference-caged particle. (f) and (g) depict the same as (b) and (c) but for the uncommon cage particles, $\Lambda(i, t_0, \Delta t)$. The white cross and red solid circle in (b)-(g) represent the mean of the probability distribution at t_0 and $t_0 + \Delta t$, respectively. The yellow arrows in (b)-(g) show the displacement direction of the reference caged particle.

tural relaxation of the fluid [22, 23]. In other words, are there any specific regions in the cage that predominantly help with cage relaxation and persistence? Note, for a reference caged-particle, say i^{th} -particle, and its cage particles $C(i, t_0)$ defined at time t_0 , a subset of these particles, $K(i, t_0, \Delta t)$, will remain part of the cage $C(i, t_0 + \Delta t)$ at later time $t_0 + \Delta t$. This common subset, $K(i, t_0, \Delta t) = C(i, t_0) \cap C(i, t_0 + \Delta t)$, contributes to cage persistence, while particles that were part of $C(i, t_0)$ but are not included in $C(i, t_0 + \Delta t)$, denoted as $\Lambda(i, t_0, \Delta t) = C(i, t_0) \setminus C(i, t_0 + \Delta t)$, contribute to cage breaking [Fig. 3(a)]. Here, “\” denotes the set difference.

To investigate if particles in certain spatial regions of the cage are more likely to contribute to cage persistence, we analyze $P(\mathbf{r}_j^{disp}(t_0)|k_j \in K(i, t_0, \Delta t))$ and $P(\mathbf{r}_j^{disp}(t_0 + \Delta t)|k_j \in K(i, t_0, \Delta t))$. We find that at t_0 , particles that are located in the direction of the displacement of the reference caged-particle have a higher likelihood of remaining part of the cage of the same particle at $t_0 + \Delta t$ [Fig. 3(b) & Supplemental Video 3]. At $t_0 + \Delta t$, however, the common particles of the cage at t_0 and $t_0 + \Delta t$ are more likely to be found in the transverse direction of the reference-cage particle [Fig. 3(c) & Supplemental Video 3]. To further corroborate these arguments, we have only considered a subset of $K(i, t_0, \Delta t)$ such that they lie within an angular region of $\pm 15^\circ$ with respect to the direction of displacement of the reference-cage particle. Figure 3(d) and (e) clearly show that common cage particles rearrange in a distinctive “mushroom cloud” pattern, rearranging their positions vertically and moving opposite to the direction of the reference caged-particle’s displacement. Conversely, the uncommon particles of the cage, initially distributed opposite to the displacement direction at t_0 , become more diffused at $t_0 + \Delta t$ [Fig. 3(f)-(g) & Supplemental Video 3]. This indicates that cage breaking and structural relaxation are predominantly facilitated by particles of the cage that are in the regions opposite the reference caged-particle’s motion.

In summary, our experiments represent a first-of-its-kind unravelling of the microscopic dynamics of cage evolution, consistent with unique features of emergent near-field hydrodynamic interactions for q2D colloidal fluids. We demonstrate cages evolve isotropically and symmetrically in the laboratory frame of reference. However, ensemble-averaged analyses reveal anisotropic and asymmetric evolution in the displacement frame of the reference caged-particle. Colloids forming the cage, which are initially ahead of the reference caged-particle, reorganize and diffuse transversely with respect to the direction of displacement of the caged-particle, contributing to the persistence of the cage. Conversely, particles behind the reference caged-particle diffuse further away, predominantly leading to cage breaking and structural relaxation of the fluid. While our study focussed on cage

dynamics for colloidal fluids in 2D rigid confinement, it would be worthwhile to explore them for suspension of particles at interfaces [16, 27] as well as ones confined on curved surfaces [28, 29]. Additionally, future studies may explore systems with broken ergodicity, such as jammed and glassy states [30–32], active matter that may have non-trivial cage relaxation dynamics [33], and systems with soft and anisotropic particles that will introduce ruggedness in the energy landscapes, even in two dimensions [34–36].

We are grateful for the useful discussions with Siva-surender Chandran, B. Prasanna Venkatesh, and K. Hima Nagamanasa. We gratefully acknowledge financial support from the Department of Science and Technology (Government of India), INSPIRE fellowship IF200274 (N.H.B.), research initiation grant from IIT Gandhinagar through IP/IITGN/PHY/CM/2021/11 (C.K.M.) and the Start-up Research Grant of Science and Engineering Research Board of Government of India through SRG/2021/001077 (C.K.M.).

* chandan.mishra@iitgn.ac.in

- [1] P. M. Reis, R. A. Ingale, and M. D. Shattuck, Caging dynamics in a granular fluid, *Phys. Rev. Lett.* **98**, 188301 (2007).
- [2] F. Perakis, G. Camisasca, T. J. Lane, A. Späh, K. T. Wikfeldt, J. A. Sellberg, F. Lehmkuhler, H. Pathak, K. H. Kim, K. Amann-Winkel, *et al.*, Coherent X-rays reveal the influence of cage effects on ultrafast water dynamics, *Nat. Communications* **9**, 1917 (2018).
- [3] N. Giri, M. G. Del Pópolo, G. Melaugh, R. L. Greenaway, K. Rätzke, T. Koschine, L. Pison, M. F. C. Gomes, A. I. Cooper, and S. L. James, Liquids with permanent porosity, *Nature* **527**, 216 (2015).
- [4] P. Gallo, F. Sciortino, P. Tartaglia, and S.-H. Chen, Slow dynamics of water molecules in supercooled states, *Phys. Rev. Lett.* **76**, 2730 (1996).
- [5] B. Li, K. Lou, W. Kob, and S. Granick, Anatomy of cage formation in a two-dimensional glass-forming liquid, *Nature* **587**, 225 (2020).
- [6] G. Marty and O. Dauchot, Subdiffusion and cage effect in a sheared granular material, *Phys. Rev. Lett.* **94**, 015701 (2005).
- [7] E. R. Weeks and D. Weitz, Properties of cage rearrangements observed near the colloidal glass transition, *Phys. Rev. Lett.* **89**, 095704 (2002).
- [8] G. Parisi and F. Zamponi, Mean-field theory of hard sphere glasses and jamming, *Rev. Mod. Phys.* **82**, 789 (2010).
- [9] E. Rabani, J. D. Gezelter, and B. Berne, Direct observation of stretched-exponential relaxation in low-temperature Lennard-Jones systems using the cage correlation function, *Phys. Rev. Lett.* **82**, 3649 (1999).
- [10] S. L. White, P. Banerjee, and P. K. Jain, Liquid-like cationic sub-lattice in copper selenide clusters, *Nature Communications* **8**, 14514 (2017).
- [11] R. Quinn and J. Goree, Particle interaction measurements in a Coulomb crystal using caged-particle motion, *Phys. Rev. Lett.* **88**, 195001 (2002).
- [12] S. J. Gerbode, D. C. Ong, C. M. Liddell, and I. Cohen, Dislocations and vacancies in two-dimensional mixed crystals of spheres and dimers, *Phys. Rev. E* **82**, 041404 (2010).
- [13] C. Mayer, E. Zaccarelli, E. Stiakakis, C. Likos, F. Sciortino, A. Munam, M. Gauthier, N. Hadjichristidis, H. Iatrou, P. Tartaglia, *et al.*, Asymmetric caging in soft colloidal mixtures, *Nat. Materials* **7**, 780 (2008).
- [14] V. E. Debets, X. M. De Wit, and L. M. Janssen, Cage length controls the nonmonotonic dynamics of active glassy matter, *Phys. Rev. Lett.* **127**, 278002 (2021).
- [15] H. Zhang, Q. Zhang, F. Liu, and Y. Han, Anisotropic-isotropic transition of cages at the glass transition, *Phys. Rev. Lett.* **132**, 078201 (2024).
- [16] B. Illing, S. Fritschi, H. Kaiser, C. L. Klix, G. Maret, and P. Keim, Mermin-wagner fluctuations in 2D amorphous solids, *Proc. Natl. Acad. Sci. USA* **114**, 1856 (2017).
- [17] S. Vivek, C. P. Kelleher, P. M. Chaikin, and E. R. Weeks, Long-wavelength fluctuations and the glass transition in two dimensions and three dimensions, *Proc. Natl. Acad. Sci. USA* **114**, 1850 (2017).
- [18] X. Zheng and J. Earnshaw, On the Lindemann criterion in 2D, *Europhys. Lett.* **41**, 635 (1998).
- [19] Y.-W. Li, C. K. Mishra, Z.-Y. Sun, K. Zhao, T. G. Mason, R. Ganapathy, and M. Pica Ciamarra, Long-wavelength fluctuations and anomalous dynamics in 2-dimensional liquids, *Proc. Natl. Acad. Sci. USA* **116**, 22977 (2019).
- [20] H. Shiba, T. Kawasaki, and K. Kim, Local density fluctuation governs the divergence of viscosity underlying elastic and hydrodynamic anomalies in a 2d glass-forming liquid, *Phys. Rev. Lett.* **123**, 265501 (2019).
- [21] N. H. Barbhuiya, A. Yodh, and C. K. Mishra, Direction-dependent dynamics of colloidal particle pairs and the Stokes-Einstein relation in quasi-two-dimensional fluids, *Nat. Communications* **14**, 5109 (2023).
- [22] Y. Chen, Z. Ye, K. Wang, J. Huang, H. Tong, Y. Jin, K. Chen, H. Tanaka, and P. Tan, Visualizing slow internal relaxations in a two-dimensional glassy system, *Nat. Phys.* **19**, 969 (2023).
- [23] X. Cao, H. Zhang, and Y. Han, Release of free-volume bubbles by cooperative-rearrangement regions during the deposition growth of a colloidal glass, *Nat. Communications* **8**, 362 (2017).
- [24] J. C. Crocker and D. G. Grier, Methods of digital video microscopy for colloidal studies, *J. Colloid Interface Sci.* **179**, 298 (1996).
- [25] P. A. Burrough, R. A. McDonnell, and C. D. Lloyd, *Principles of geographical information systems* (Oxford University Press, USA, 2015).
- [26] Method for determining the inner contour of the probability distribution's maxima through ray tracing: Rays are emanated in all directions and traced from the probability distribution's center (mean) to identify points where the probability exceeds $\sim 95\%$ of the maximum probability. These points define the contour on which an ellipse is fitted.
- [27] C. van Baalen, J. Vialetto, and L. Isa, Tuning electrostatic interactions of colloidal particles at oil-water interfaces with organic salts, *Phys. Rev. Lett.* **131**, 128202 (2023).
- [28] A. Bausch, M. J. Bowick, A. Cacciuto, A. Dinsmore, M. Hsu, D. Nelson, M. Nikolaidis, A. Travestet, and

- D. Weitz, Grain boundary scars and spherical crystallography, *Science* **299**, 1716 (2003).
- [29] N. Singh, A. Sood, and R. Ganapathy, Observation of two-step melting on a sphere, *Proc. Natl. Acad. Sci. USA* **119**, e2206470119 (2022).
- [30] P. Charbonneau, A. Ikeda, G. Parisi, and F. Zamponi, Dimensional study of the caging order parameter at the glass transition, *Proc. Natl. Acad. Sci. USA* **109**, 13939 (2012).
- [31] P. Charbonneau, Y. Jin, G. Parisi, and F. Zamponi, Hopping and the Stokes-Einstein relation breakdown in simple glass formers, *Proc. Natl. Acad. Sci. USA* **111**, 15025 (2014).
- [32] P. K. Morse and E. I. Corwin, Geometric signatures of jamming in the mechanical vacuum, *Phys. Rev. Lett.* **112**, 115701 (2014).
- [33] R. Ni, M. A. C. Stuart, and M. Dijkstra, Pushing the glass transition towards random close packing using self-propelled hard spheres, *Nat. Communications* **4**, 2704 (2013).
- [34] X. Yang, R. Liu, M. Yang, W.-H. Wang, and K. Chen, Structures of local rearrangements in soft colloidal glasses, *Phys. Rev. Lett.* **116**, 238003 (2016).
- [35] Z. Zheng, F. Wang, and Y. Han, Glass transitions in quasi-two-dimensional suspensions of colloidal ellipsoids, *Phys. Rev. Lett.* **107**, 065702 (2011).
- [36] C. K. Mishra and R. Ganapathy, Shape of dynamical heterogeneities and fractional Stokes-Einstein and Stokes-Einstein-Debye relations in quasi-two-dimensional suspensions of colloidal ellipsoids, *Phys. Rev. Lett.* **114**, 198302 (2015).